Pergamon

Journal of Structural Geology, Vol. 17, No. 11, pp. 1523 to 1533, 1995

0191-8141/95 $9.50+0.00

0191-8141(95)00060-7

Comparative rheological behaviour of albite and quartz in siliceous schists revealed by the microboudinage of piedmontite

TOSHIAKI MASUDA,* TOMOKI SHIBUTANI† and HARUKA YAMAGUCHI

Institute of Geosciences, Schizuoka University, Shizuoka 422, Japan

(*Received* 15 *October* 1993; *accepted in revised form* 24 *March* 1995)

Abstract—This paper presents a detailed comparison of the microboudinage of piedmontite in two different mineralogical hosts, a quartz matrix, and albite porphyroblasts in a siliceous schist, with the aim of clarifying the rheological properties of albite in relation to those of quartz. Stress and strain analyses of the microboudinage confirm that the boudinage took place in the retrograde stage of metamorphism during decreasing temperature, and reveal that albite deformed at the same strain rate as quartz above the plastic–brittle transition temperature of albite.

INTRODUCTION

Quartz and albite are common rock-forming minerals, and their rheological behaviours are critical for deformation in the crust. It is well known that quartz flows plastically during deformation under metamorphic conditions, whereas flow of albite seems to be less common. Albite typically occurs as porphyroblasts embedded in a finer-grained matrix, in a wide variety of low-grade metamorphic rocks such as pelitic, psammitic, siliceous and basic schists. Such albite porphyroblasts usually contain various inclusions, whose geometric arrangement and mineral composition sometimes differ from those outside the porphyroblasts. The fact that the included structures are different from structures outside the porphyroblast is usually attributed to the mechanical rigidity and chemical inactivity of albite: in other words, the fabric and minerals, once enclosed in albite porphyroblasts, are interpreted to have been protected from subsequent deformation and metamorphism which has greatly rearranged or completely obliterated their counterparts outside the porphyroblasts (e.g. Zwart 1962, Vernon 1989, Yardley 1989). Thus, the included minerals in porphyroblasts provide indispensable clues to early deformation and metamorphic history. However, plagioclase is also deformable, as revealed by high *P–T* deformation experiments (e.g. Tullis & Yund 1985, 1987, 1991) and natural fabric analysis (e.g. White & Mawer 1986, Ji & Mainprice 1988). Therefore, interpretation based on rigidity of albite porphyroblasts may be wrong. We have to consider the plastic flow of albite to understand better the porphyroblast microstructures seen in metamorphic tectonites.

This paper addresses the rheology of albite by stress and strain analyses of microboudinage of piedmontite grains in a siliceous schist that deformed during high-pressure metamorphism. Columnar piedmontite grains are microboudinaged in a quartz matrix, while piedmontite grains in albite porphyroblasts are also microboudinaged. The paper analyses, in detail, the microboudinage in both the quartz matrix and albite porphyroblasts and, by comparing them draws conclusions regarding the mechanical behaviour of albite in contrast to that of quartz.

MATERIAL STUDIED

The Yamagami metamorphic rocks from which the material studied was collected are distributed in only a small area surrounded by Cretaceous granitic rocks and Mesozoic and Cenozoic strata in the northeast Abukuma Plateau, Japan (Iwamatsu 1975, for locality see also Masuda *et al.* 1989, 1990). They consist of basic, pelitic, psammitic and siliceous schists, and they underwent glaucophane-schist facies and epidote–amphibolite facies metamorphism (Kuroda & Ogura 1963, Maekawa 1988). The age of the metamorphism is considered to be pre-Late Devonian (Iwamatsu 1975, Hara & Umemura 1979).

The siliceous schist studied has a foliation defined by a parallel arrangement of mica flakes, and a lineation on the foliation surface defined by the linear arrangement of columnar piedmontite grains. The foliation is undulatory at the hand-specimen scale. The schist is the same as that analysed in Masuda *et al.* (1989, 1990).

MICROSTRUCTURE

Using the optical microscope, detailed observations were made on thin sections cut perpendicular to the foliation and parallel to the lineation. The sample consists mainly of quartz matrix plus albite, with minor amounts of piedmontite, muscovite, garnet, tourmaline, apatite and opaque minerals.

*Present address: Department of Earth Sciences, James Cook University of North Queensland, Townsville Q4811, Australia.

†Present address: Power Reactor and Nuclear Fuel Development Corporation, Tokaimura, Ibaraki 319-11, Japan.

Piedmontite grains occur both in the quartz matrix and in albite porphyroblasts (Fig. 1). The piedmontite grains are more or less columnar, with both ends tapered. Their width is usually less than 0.1 mm and their length less than 0.3 mm. They are microboudinaged with the fracture planes of the microboudins oriented almost perpendicularly to the lineation, while the separation follows the lineation either exactly or at least approximately. This indicates that no observable rotation of the microboudins took place during the microboudinage and suggests that deformation is of nearly pure shear type with no strong simple shear component (e.g. Ramberg 1955, Ramsay 1967 pp. 221–226, Ghosh & Ramberg 1976, Hossain 1979, Hanmer 1986, Masuda *et al.* 1995). The fracture planes are relatively sharp, and no ductile deformation is apparent at their edges, suggesting that the competence contrast between piedmontite and quartz or albite was large when the microboudinage took place (e.g. Ramberg 1955, Ramsay 1967 pp. 103–106, Lloyd *et al.* 1982). The piedmontite grains show various stages of microboudinage; some grains are unbroken, some have just started to separate into two microboudins, and some are pulled apart remarkably far. Many broken grains are separated into two or three segments, and a few into six–nine. Inter-boudin gaps in the quartz matrix are usually occupied by polycrystalline quartz, but sometimes by single quartz grains. Those in albite porphyroblasts are usually occupied by single albite grains.

Albite forms porphyroblasts surrounded by a quartz matrix, its mode being approximately 3%. Many albite porphyroblasts occur in albite-rich layers that are parallel to the foliation. The porphyroblasts are ovoid or lenticular in shape, with their longest axes parallel to the foliation. One large one (Figs. 1d–g) is described in detail here, because all the piedmontite grains used for the microboudinage analysis are enclosed in it. Thus, the strain rate of albite discussed in later sections only concerns this porphyroblast. Its size is exceptionally large: the width is 2.8 mm, and the length is 12 mm, with the aspect ratio being 4.3. Its periphery is not smoothly curved but ragged in places. It consists of many albite grains of irregular shape, the grain boundaries appearing straight but, on a closer look, most such boundaries are serrated or jagged. These grains commonly show slight to moderate undulatory extinction. Neoblasts, presumably produced by dynamic recrystallization, seldom occur in them. Neither deformation bands nor lamellae were detected. The porphyroblast also contains inclusions of tourmaline, apatite and opaque minerals other than piedmontite. In its centre, a lenticular quartz aggregate occurs, the longest axis of which is 0.45 mm and parallel to the foliation: the shortest axis being 2.3 mm. The aspect ratio of the lenticular quartz aggregate is 4.1, which is similar to that of the host albite porphyroblast. This porphyroblast itself was fractured and pulled apart (boudinaged). The pulled-apart gaps are occupied by quartz. Two sets of fracture planes occur highly oblique to the foliation (Figs. 1e & g) and are presumably conjugate. The orientations of the principal stresses for pull-apart of the albite porphyroblast are consistent with those for the microboudinage of piedmontite.

Other albite porphyroblasts are usually 0.5–1.5 and 3–5 mm in width and length, respectively, with aspect ratios ranging between 2 and 5. They consist of single albite grains or albite aggregates. They often show pull-apart (microboudinage) structures filled with quartz, with the fracture planes oriented perpendicular to the foliation plane (Fig. 1b). Some fracture planes are conjugate. Most albite porphyroblasts show slight undulatory extinction and contain no dynamically recrystallized neoblasts. Neither deformation bands nor lamellae were detected.

Plastic deformation of the albite porphyroblasts appears heterogeneous, because the intensity of piedmontite microboudinage varies from porphyroblast to porphyroblast. This variation is probably due to the different crystallographic orientations of albite with respect to the principal stress axes. The piedmontite microboudinage appears most intense in the analysed large porphyroblast. The intensity of undulatory extinction also suggests that the large porphyroblast is more strained.

The quartz matrix, appearing very heterogeneous (Fig. 1c), mostly consists of relatively large elongate ribbon grains. The elongation of the ribbon grains is parallel to the foliation. Their aspect ratios usually range from 3 to 10, but in a few cases exceed 15. The width and length of typical ribbon grains range from 0.01 to 0.2 mm and from 0.1 to 1 mm, respectively, although their exact shape cannot be depicted because of ubiquitous strong undulatory extinction and the common occurrence of small, equant neoblasts along grain boundaries. Grain boundaries of elongate grains are highly serrated, even where no neoblasts exist. Neoblasts also occur within elongate grains. The diameter of neoblasts, both along grain boundaries and within grains, is 0.01 mm on average. Equant, equigranular quartz aggregates are

Fig. 1. Photomicrographs of the piedmontite-bearing quartz schist in a plane parallel to the lineation and perpendicular to the foliation; p = piedmontite; q = quartz; a = albite. Foliation in (a) is oriented upper-right to lower-left, in (b)–(f) it is sub-parallel to the base of the photos. (a) Piedmontite boudins parallel to the lineation in a quartz matrix (plane polarized light). (b) Boudinaged albite porphyroblast that includes piedmontite, apatite and opaque mineral (plane polarized light). Fractures are perpendicular to the foliation. Inter-boudin gaps, indicated by arrows, are filled with quartz. The foliation deflects around the porphyroblast. (c) Elongate quartz grains parallel to the foliation (crossed nicols). (d) Large albite porphyroblasts used in the analysis (plane polarized light). (e) Same as (d) (crossed nicols). Conjugate boudin gaps in albite indicated by arrows are filled with quartz. (f) Close-up view of (d). Note tourmaline and opaque grains in addition to piedmontite. Many piedmontite and opaque grains show microboudinage structure. The long axes of these grains are aligned parallel to the foliation. (g) Same as (f) (crossed nicols). Arrows indicate conjugate fractures in the albite porphyroblasts. The conjugate boudin gaps in the albite are filled with quartz.

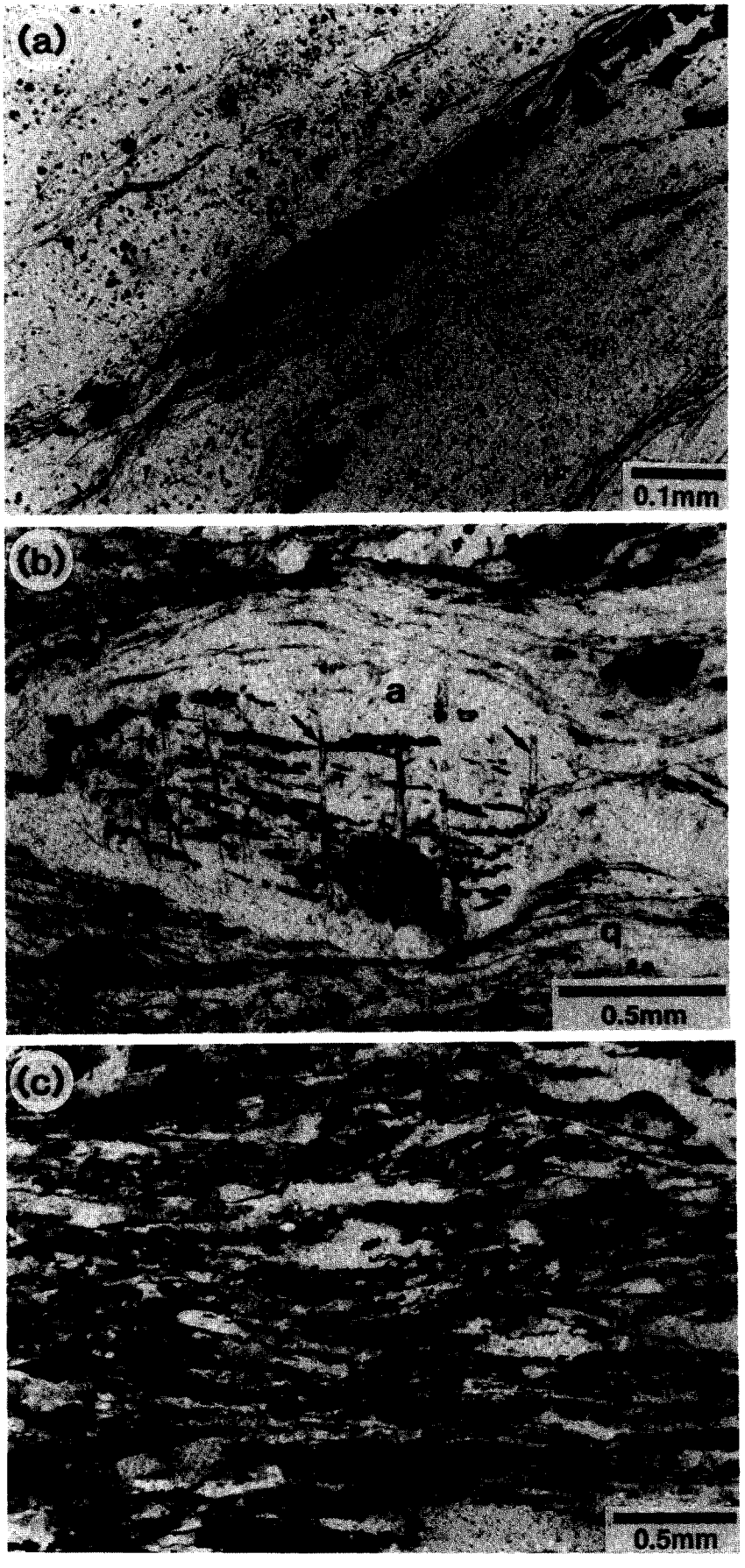
(a)
0.1mm
(b)
a
q
0.5mm
(c)
0.5mm

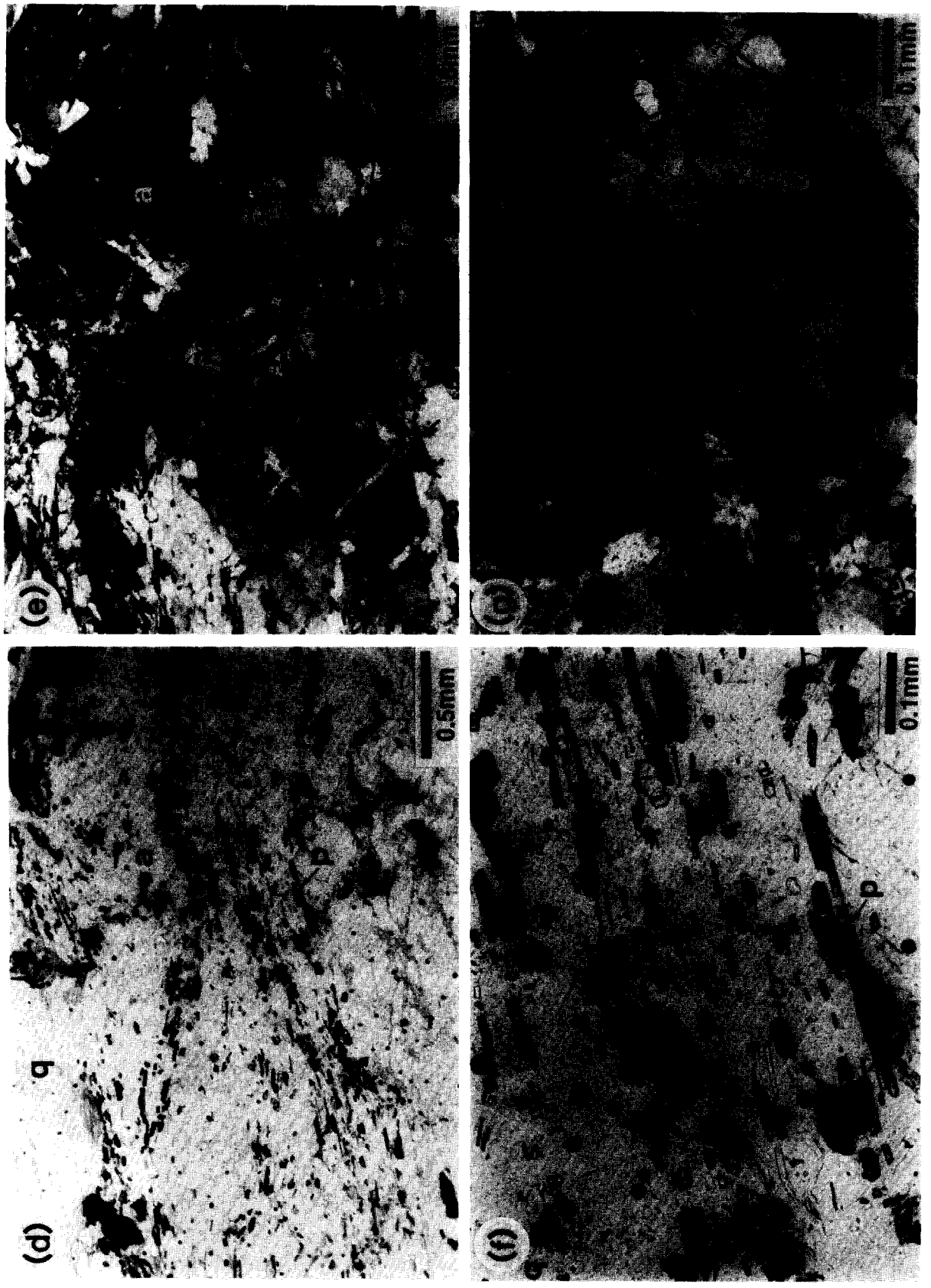
(a)
0.1mm
(b)
0.1mm
(d)
0.5mm
b
(c)
0.1mm
p

also constituents (<2 area %) of the quartz matrix, usually forming domains that are elongate parallel to the foliation. The diameter of equant grains in these domains ranges from less than 0.01–0.03 mm. These grains hardly show undulatory extinction or other deformation features such as deformation lamellae and deformation bands. As we did not make observations using transmission electron microscopy, these quartz grains cannot be correlated well with grains studied by Hirth & Tullis (1992). In optical appearance, however, homogeneously elongate grains are most similar to grains of Regime 2 microstructures of Hirth & Tullis (1992), although the absence of deformation lamellae in our schist is not consistent with Regime 2 microstructures. Our grains are also similar to elongate grains of S-type microstructure described by Masuda & Fujimura (1981).

PHYSICAL BASIS OF THE METHOD

We analysed both strain and stress using the method proposed by Masuda *et al.* (1989, 1990). The method deals with microboudinage, which consists of two different processes: brittle fracturing of a competent material and subsequent separation of boudins. Fracturing is related to differential stress that is transferred to competent materials through elastic constants (fibre-loading theory: e.g. Kelly 1973, Lloyd *et al.* 1982, Ferguson & Lloyd 1982, Ji & Zhao 1993). On the other hand, subsequent separation of boudins is related to plastic flow of the matrix. Thus, microboudinage is a complex product of brittle, elastic and plastic behaviour of minerals. In Masuda & Kuriyama (1988) and Masuda *et al.* (1989, 1990) we inferred that the microboudinage was proceeded by 'viscoelastic' behaviour of the matrix material. This inference is wrong: we now realize that 'viscoelastic' should be replaced by 'plastic–elastic', because quartz and albite were never molten but were in a solid-state condition during metamorphism. This earlier wrong interpretation does not affect the quantitative data of our previous stress and strain analyses.

MEASUREMENT OF THE PIEDMONTITE GRAINS

The method needs the aspect ratios of broken and intact competent materials as input data. In the present case, the competent material is piedmontite and the surrounding, less competent material is quartz or albite. Measurements were done in a section parallel to the lineation and perpendicular to the foliation. We measured the lengths and widths of the intact grains of piedmontite, and calculated aspect ratio as length/width. When the piedmontite grains were microboudinaged, we measured the length and width of each boudin and each gap length, and calculated the aspect ratio as shown in Fig. 2. In this measurement, we judged grains as being microboudinaged only when interboudin gaps could be observed to be filled with quartz or albite. The measurements have two types of error. If an interboudin gap is very large, we may judge the boudins as two intact grains. If it is too short to be detected under the optical microscope, we also judge them as one intact grain. The minimum detected gap distance of our measurements is approximately 0.5 μm. The measured grains numbered 586 in the quartz matrix and 317 in the large albite porphyroblast. Grains in the quartz matrix include 301 previously measured grains (Masuda *et al.* 1989, 1990) and 285 newly measured grains. Since the larger number of measured grains leads to a more reliable stress analysis (see Appendix A), the present analysis is more reliable than the previous one. Grains in the albite porphyroblast had not previously been measured. Frequency distributions of width, length and aspect ratio of restored and intact grains are shown in Fig. 3. It is apparent from this that the lengths and widths of piedmontite grains in the quartz matrix are obviously larger than those in the albite porphyroblast, but the aspect ratio is similar. Some piedmontite grains in the albite porphyroblast were 'accidentally' fractured and separated during fracturing and separation of the host albite porphyroblast. Such piedmontite grains are regarded as intact.

RESULTS OF THE STRAIN AND STRESS ANALYSES

Strain

For microboudinaged grains, we can restore the history of fracturing and separation by using the boudin lengths and gap distances with the help of the strain reversal method proposed by Ferguson (1981) (see also Ferguson & Lloyd 1984, Ferguson 1987, Lloyd & Ferguson 1989). The method provides us with the aspect ratio of each grain at the time of fracturing and the strain that contributed to the gap developed after fracturing (Fig. 4). Note that inverse natural strain (ε_{inv}), plotted on the abscissa of Fig. 4, shows the relative time of fracturing, with time increasing to the right. Its magnitude is the same as natural strain obtained by the strain reversal method, and its sign is negative. However, it is not

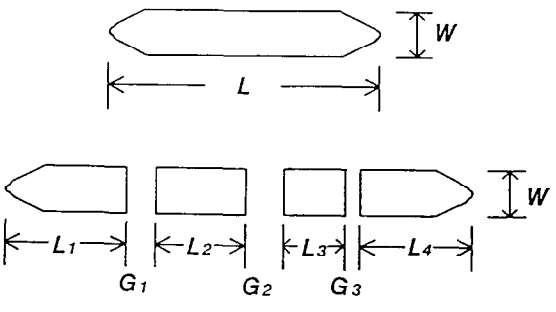

Fig. 2. Measurements on whole (top) and microboudinaged grains (bottom). L = length; W = width. The aspect ratio r is calculated as $r = L/W$. The length of the bottom grain is calculated as ΣL_i, where L_i is the length of ith boudin. All the lengths and gaps are used to restore the history of microboudinage by the strain reversal method.

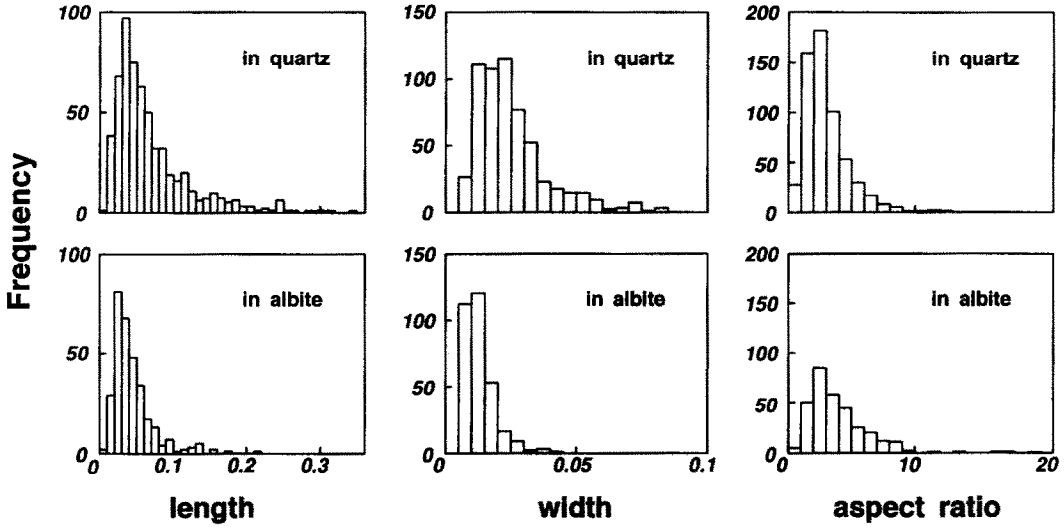

Fig. 3. Frequency distributions of length, width and aspect ratio of piedmontite grains in the quartz matrix and in the albite porphyroblast. Note that there is a wider range of distribution of length and width of the piedmontite grains in the matrix than in the albite porphyroblast. The frequency distributions of aspect ratio are more or less similar.

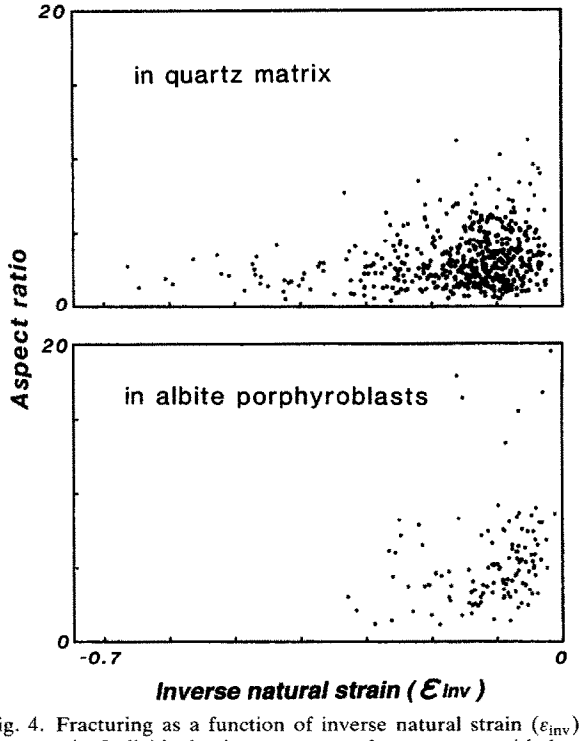

Fig. 4. Fracturing as a function of inverse natural strain (ε_{inv}) and aspect ratio. Individual points represent a fracture event with the grain aspect ratio at fracture as ordinate and the strain recorded by the gap (inverse natural strain) as abscissa. The origin on the abscissa (inverse natural strain = 0) indicates the state at which quartz or albite ceased to flow. Time increases to the right. Unbroken grains are not plotted.

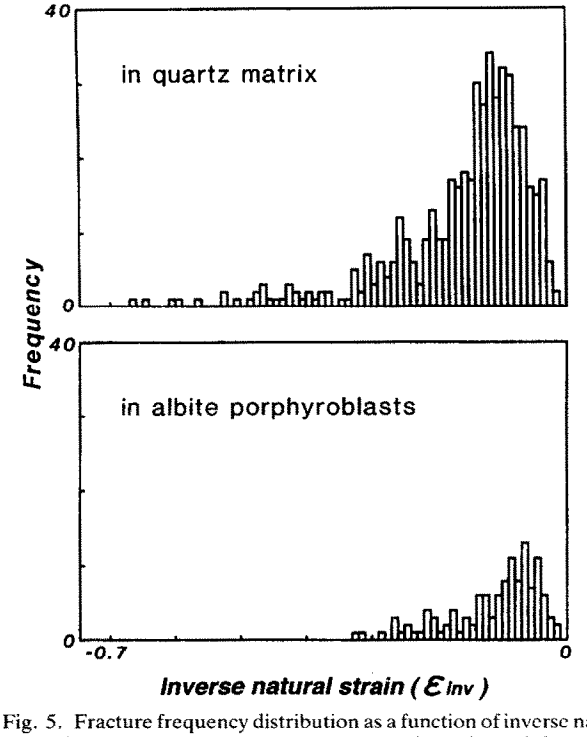

Fig. 5. Fracture frequency distribution as a function of inverse natural strain (ε_{inv}). The frequency is not uniform throughout deformation. Most fractures occurred late.

exactly proportional to time, since strain rate was definitely not constant throughout the microboudinage history. An inverse natural strain of zero represents the time at which the matrix (quartz and albite) ceased to deform plastically. If the plastic–brittle transition for albite and quartz took place at different stages of the deformation, the time when inverse natural strain reached zero for albite would be different from that for quartz. It should also be noted that the strain rate of quartz under the given conditions was possibly different from that of albite. Thus, the times taken for quartz and albite to undergo a certain strain would in general be different. There are fewer plotted points in Fig. 4 for albite than for quartz as host to the piedmontite grains. This is due to both the number of measured grains and the intensity of microboudinage. The range of inverse natural strain during microboudinage is clearly wider for piedmontite grains in the quartz matrix. However, the aspect ratios at the time of fracturing are similar for both groups of grains: most range from 1 to 8.

Figure 5 shows the fracture frequency distribution with respect to inverse natural strain. For both groups of grains, most fracturing took place in the later stages of plastic deformation. The shape of the frequency distribution is similar for both groups, although the relative

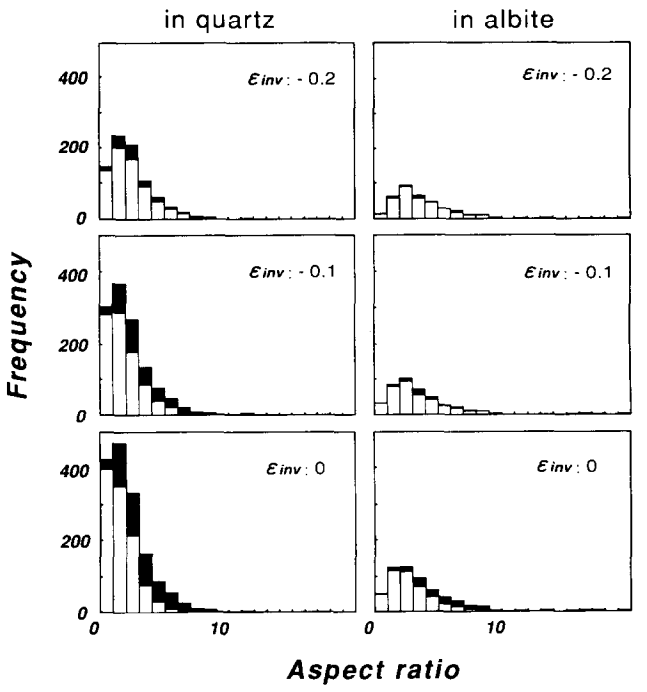

Fig. 6. Frequency distributions of grains and grain fragments with different aspect ratios at particular stages of microboudinage. Black columns represent broken grains; white columns, unbroken grains; ε_{inv} = inverse natural strain. Note that the frequencies at different inverse natural strains are different, because many fragmentary grains were produced by microboudinage.

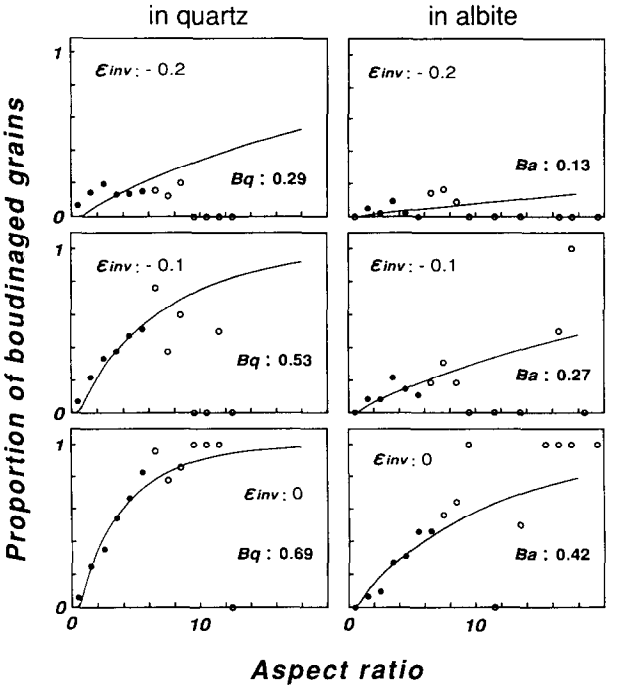

Fig. 7. Proportion of microboudinaged grains as a function of aspect ratio at distinct stages of microboudinage. This proportion generally increases with increasing aspect ratio. The data are considered reliable when the total number of measured grains exceeds 25. Full circles show reliable data, open circles unreliable data. The values of B_a and B_q and curves of best fit for the reliable data have been predicted theoretically (see text).

frequency is different. The peak frequency was recorded at inverse natural strains of -0.12 and -0.07, respectively, for grains in the quartz matrix and in the albite porphyroblast. This mismatch is important in our later discussion.

Stress

Following Masuda *et al.* (1990), we can count previously existing and broken grains during the history of microboudinage as well as grains (including microboudins) now observed. Thus, it is possible to obtain the number of broken and intact grains as a function of aspect ratio at any inverse natural strain. The cumulative number of grains in Fig. 6 is, therefore, very different from the number of grains shown in Fig. 3. From Fig. 6, we can obtain the proportion of broken grains with respect to aspect ratio, as shown in Fig. 7. This gives the basic data needed for estimating the relative value of differential stress, with the method proposed by Masuda *et al.* (1989).

The method assumes a homogeneous deformation in the sample, and involves: (1) measurement of the proportion of broken grains in relation to their aspect ratio; (2) the theoretical prediction of that proportion as a function of the parameter $B = (E_f/E_m)\ (S_{bulk}/S^*)$, where E_f and E_m are Young's modulus of boudin and surrounding matrix, respectively, S^* is the mean fracture strength of the boudinaged material with unit aspect ratio, and S_{bulk} is the differential stress imposed on the rock body; and (3) a search for the best-fit value of B that minimizes the square of the difference between the measured and predicted proportions. As indicated above, the measured proportions for the sample are shown in Fig. 7. The theoretical proportion of broken to whole grains, G, for a given aspect ratio, r, is expressed by the equation:

$$G(r, B) = 1 - \exp\left[-\frac{m-1}{m} rB^m\left(1 - \frac{1}{\cosh(Ar)}\right)^m\right],$$

where m and A are constants (Masuda *et al.* 1989). For a best fit of B, we need the value of m and A. These were determined by Masuda *et al.* (1989) as 2 and 2.2, respectively. The measured proportions are considered as reliable when the number of measurements exceeds 25 (Appendix A). Only reliable data thus defined were used for determining the best-fit value of B. Uncertainty in estimating B is usually less than $\pm$ 0.1 (Appendix A). In practice, since we have two different materials surrounding the piedmontite, B was redefined as B_q and B_a for the quartz matrix and albite porphyroblast, respectively. The determined best-fit values of B (B_q and B_a) and the theoretically predicted curves are shown in Fig. 7 for distinct stages of deformation in each group of grains. After determining the values of B_q and B_a for other stages of deformation, we obtain Fig. 8 which shows how the values of B_q and B_a changed with progressing microboudinage. It is evident that in the later stages of deformation, the values of B_q and B_a increase rather rapidly. This rapid increase correlates with the large late frequency of fracturing shown in Fig. 5.

DISCUSSION

Relative timing of microboudinage and albite porphyroblast formation

Since albite porphyroblasts contain piedmontite grains, their formation unambiguously postdated the appearance of piedmontite in the siliceous schist. The essential question is whether the piedmontite grains had already been microboudinaged before they were enclosed in the albite porphyroblasts. There are two possible answers: piedmontite microboudinage predated (Case 1), or postdated (Case 2) the development of the albite porphyroblasts. We prefer Case 2, for four reasons. The first is related to microstructural characteristics of the albite porphyroblasts. Since these porphyroblasts show undulatory extinction, and their shape is mostly elongate parallel to the extension direction of the microboudinage, intense deformation involving microboudinage after porphyroblast growth (Case 2) is strongly suggested.

The second reason is related to the length and width of the piedmontite grains, which are smaller in albite porphyroblasts than in the quartz matrix. This relationship is easily explained in Case 2: piedmontite grains ceased to grow when they were enclosed in the albite porphyroblasts, while those outside the porphyroblasts continued to grow. These length and width differences are hard to explain in Case 1.

The third reason is related to the stress–strain curves for albite and quartz inferred from the microboudinage analysis (Fig. 8). If we assume Case 1, the large albite porphyroblast would have developed at the time when inverse natural strain (ε_{inv}) for albite equalled zero in Fig. 8. At that time, $B_a = 0.42$ (see the ordinate at $\varepsilon_{inv} = 0$). Before the albite porphyroblast formation, microboudins now enclosed in the albite porphyroblast would have been produced in the quartz matrix. Thus, B_a and B_q would have synchronously changed until the albite porphyroblast formed. This indicates that $B_a = B_q = 0.42$ at the time of albite porphyroblast formation, and that the quartz matrix would have plastically flowed by a natural strain of 0.13 after the albite porphyroblast formation (see the abscissa when $B_q = 0.42$ of Fig. 8). This view requires that the two curves for B_a and B_q in Fig. 8 should be the same if strain for B_a is shifted by 0.13 backwards on the abscissa. However, the shifted B_a curve does not well fit to the B_q curve, especially for B_a and B_q larger than 0.3. This does not support Case 1.

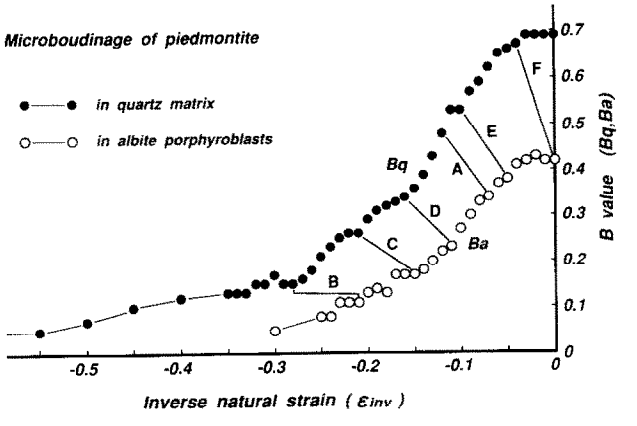

Fig. 8. Best-fit values of B (B_a and B_q) with respect to inverse natural strain (ε_{inv}). Both B_a and B_q increase with increasing time. Tie lines A–F connect synchronous points for quartz and albite. The reason why they are considered synchronous is presented in the text.

The fourth reason is related to the frequency of fracturing with respect to inverse natural strain (Fig. 5). If we assume Case 1, fracturing of the piedmontite now included in the albite porphyroblast would also have occurred in quartz, and quartz would have flowed by a strain of 0.13 after the albite porphyroblast formation, as stated above. Since the peak frequency of fracturing in the albite occurs at $\varepsilon_{inv} = -0.07$, a local peak frequency of fracturing in the quartz matrix should occur at $\varepsilon_{inv} = -0.20$ ($= -0.13$–0.07), owing to the synchronous rapid increase in differential stress in quartz matrix and the albite porphyroblast (see (1) of the next section). However, no clear local peak frequency can be detected at this strain in Fig. 5. Thus, Fig. 5 is difficult to account for in Case 1. On the other hand, the B_a and B_q curves in Fig. 8 and frequency of fracturing in Fig. 5 can be well explained in Case 2, as described below.

Time correlation of stress–strain curves of quartz and albite in Case 2

Figure 8 shows how the B values changed with increasing natural strain for the two host materials. The abscissa, inverse natural strain, embraces no quantitative constraint on the time for either curve on this plot. In the following, we give constraints on the time relationship between the two curves, assuming Case 2:

(1) As a consequence of a rapid increase in the external differential stress imposed on the rock body, intense fracturing of the piedmontite would have taken place in the quartz matrix. The rapid increase in differential stress was transferred to the albite and ultimately to the piedmontite grains within the albite porphyroblast, resulting in intense fracturing of piedmontite inside the albite. Thus, the peak frequency in Fig. 5 for quartz (at $\varepsilon_{inv} = -0.12$) and albite (at $\varepsilon_{inv} = -0.07$) presumably occurred at the same time. The tie-line A, bridging the two equivalent points in Fig. 8 shows this synchronism, and the ordinates of these points indicate that $B_a = 0.34$ and $B_q = 0.48$ at this time.

(2) B_a and B_q are expressed as:

$$B_a = (E_f/E_a)(S_{ab}/S^*)$$

and

$$B_q = (E_f/E_q)(S_{bulk}/S^*),$$

where E_a and E_q are elastic constants for albite and quartz, and S_{ab} is the bulk stress borne by the albite porphyroblast. Since the albite porphyroblast is embedded in the quartz matrix, the bulk stress for the albite

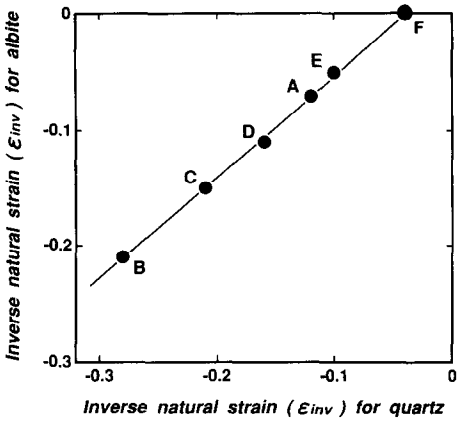

Fig. 9. Comparison of natural strain in quartz and albite. Each point (A–F) represents the synchronized values of inverse natural strain (ε_{inv}) for quartz and albite connected by tie-lines A–F in Fig. 8. The tangent of the regression line for points A–E indicates that quartz and albite flowed plastically at the same strain rate. Point F is plotted by extrapolation of the line to the cessation of flow of albite. See text for explanation.

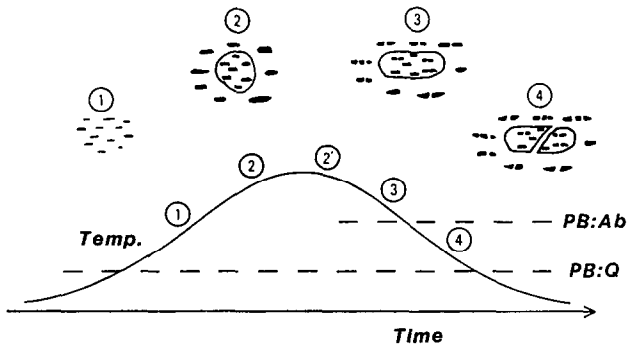

Fig. 10. Schematic history of development of microstructure during prograde and retrograde metamorphism. Stage numbers are encircled. The schematic drawing for each stage shows the microstructure of piedmontite (in black) and an albite porphyroblast. PB:Ab and PB:Q are the plastic–brittle transition temperatures for albite and quartz, respectively. See text for explanation.

porphyroblast (S_{ab}) may be described as a function of the bulk stress for the rock body, S_{bulk}. Here we assume that S_{ab} is proportional to S_{bulk} expressed as $S_{ab} = KS_{\text{bulk}}$, where K is a constant. Then $B_a = (E_f/E_a)(S_{ab}/S^*) = (E_f/E_a)(K\,S_{\text{bulk}}/S^*) = K\,(E_q/E_a)B_q$.

This equation implies that $B_a/B_q = K\,(E_q/E_a) =$ constant. Because $B_a = 0.34$ and $B_q = 0.48$ at the time of peak frequency of fracturing as described above, we can obtain the value B_a/B_q as $B_a/B_q = K\,(E_q/E_a) = 0.71$. Since B_a/B_q can be regarded as a constant in our stress analysis (see Appendix B), B_a/B_q is considered to remain constant at every moment.

(3) Considering the B_a/B_q value (= 0.71) and the attitude of the B curves in Fig. 8, at least four sets of points on the two curves were picked as representing synchronous values of B_a and B_q and inverse natural strains. These points are connected by solid tie-lines B, C, D and E in Fig. 8. They all occur where the slopes of the curves sharply change.

(4) Based on the above-correlated, five tie-lines (A–E) in Fig. 8, we can compare how much strain quartz and albite experienced in a specific period of time, as shown in Fig. 9. This figure indicates that nearly the same strain was developed by the quartz and the albite in the same length of time, which thus demonstrates that the strain rates of the two materials were nearly the same.

(5) Considering the above-correlated five sets of points in Fig. 8, and extrapolating the same strain rate for quartz and albite to the ending of plastic deformation of albite (Fig. 9), another tie-line can be drawn between an inverse natural strain of −0.04 for quartz and 0 for albite (tie-line F in Fig. 8). This correlation indicates that $B_q = 0.67$ and $B_a = 0.42$ when albite ceased to flow, and that quartz still flowed plastically by a natural strain of 0.04 after albite became brittle. The final value of the ratio B_a/B_q is considerably smaller than 0.71. This is presumably related to the difficulty in judging the microboudinage of grains just started to separate in the albite porphyroblast. B_a at $\varepsilon_{\text{inv}} = 0$ is presumably undervalued.

Timing of piedmontite microboudinage

Here we discuss another question of the timing of the microboudinage: was it during prograde or retrograde metamorphism? We believe that the microboudinage took place in the retrograde stage during decreasing temperature. The reasons are as follows:

(1) Albite porphyroblasts are considered to form during prograde to early retrograde metamorphism (e.g. Itaya 1978, Takagi & Hara 1979, Otsuki 1980). As the microboudinage is considered to postdate the formation of the albite porphyroblast as discussed earlier, the microboudinage is likely to have taken place in the retrograde stage.

(2) The tie-line F (Fig. 8) indicates that quartz still continued to flow when albite had ceased to flow. This is easily explained by the retrograde microboudinage occurring during decreasing temperature (Fig. 10), because the plastic–brittle transition temperature is higher for feldspar than for quartz (e.g. Tullis & Yund 1977).

(3) If the microboudinage had taken place in the prograde stage, the schist would have experienced post-deformation annealing under amphibolite facies P–T conditions. Such annealing would have presumably destroyed the deformation microstructures. However, highly deformed quartz and albite grains actually survive in the schist, which strongly suggests no such annealing event occurred.

(4) Piedmontite grains never overgrew in the interboudin gaps (cf. Misch 1969).

Deformation of the albite porphyroblast

If the albite porphyroblast was spherical when it first appeared in the schist, we can estimate the total plastic strain that the albite porphyroblast underwent from its aspect ratio. The value of this strain is 0.73. Since the maximum extensional strain recorded by separation of piedmontite microboudines in the quartz matrix until albite became brittle is 0.66 (=0.70 − 0.04) (Fig. 5), the first fracturing of piedmontite in the quartz matrix took place when the albite had deformed by a natural strain of 0.07 (=0.73 − 0.66) after the albite porphyroblast for-

mation, accepting 0.73 for the plastic strain of albite. This value suggests that the first fracturing of piedmontite in the quartz matrix occurred shortly after the albite started to deform, whereas the first fracturing in the albite porphyroblast took place later (Figs. 4 and 5).

The quartz-filled pull-apart structure of the albite porphyroblasts is inferred to have formed after albite ceased to flow, but before quartz ceased to flow, during the latest stage of the metamorphism. The strain reversal method revealed that the boudinage of most albite grains recorded natural strains of less than 0.03. Thus quartz flowed by a natural strain of 0.03 after the albite grains brittley fractured. One exceptional albite grain (Fig. 1b) exhibits a natural strain of 0.05 after boudinage was initiated.

Summary of microstructural development of the siliceous schist

The following history of microstructural development is inferred assuming the timing of albite porphyroblast formation as in Case 2. During the prograde stage of metamorphism (stage 1 in Fig. 10), piedmontite appeared in the siliceous schist. Between stages 1 and 2, albite porphyroblasts grew rapidly, and they enclosed some piedmontite grains. Albite porphyroblasts may have continued to grow until the early retrograde stage, stage 2′. Piedmontite grains in the quartz matrix continuously grew from stage 1 to 2 or 2′, whereas those enclosed in the albite porphyroblasts ceased to grow. Between stages 2 or 2′ and 3, microboudinage began and progressed with increasing differential stress. The quartz matrix and the analysed albite porphyroblast deformed plastically at the same strain rate during this period. Other albite porphyroblasts presumably deformed at lower strain rates. Albite porphyroblasts were flattened. In stage 3, albite ceased to flow, while quartz still continued to flow. Between stages 3 and 4, albite fractured in a brittle manner resulting in (conjugate) pull-apart structures filled with quartz. At stage 4, quartz eventually ceased to flow. The plastic microstructural features were quenched at this stage.

CONCLUSIONS

For the sample of siliceous schist from Yamagami, we conclude the following:

(1) Piedmontite grains were microboudinaged after they were included in the albite porphyroblasts.

(2) The microboudinage took place in the retrograde stage of metamorphism during decreasing temperature.

(3) Above the brittle–plastic transition temperature of albite, the strain rate of the albite porphyroblast and the quartz matrix were nearly the same.

Acknowledgements—We thank C. J. Spiers and S. Yoshida for critically reading an early version of the manuscript, P. J. Hudleston and anonymous referees for improving the manuscript, and G. E. Lloyd and C. C. Ferguson for their opinions on boudinage which stimulated us and guided our analysis. This work was financially supported by the Japanese Ministry of Education.

REFERENCES

Cheeney, R. F. 1983. *Statistical Methods in Geology*. George Allen & Unwin, London.

Ferguson, C. C. 1981. A strain reversal method for estimating extension from fragmented rigid inclusions. *Tectonophysics* **79**, T43–T52.

Ferguson, C. C. 1987. Fracture and separation histories of stretched belemnites and other rigid-brittle inclusions in tectonites. *Tectonophysics* **139**, 255–273.

Ferguson, C. C. & Lloyd, G. E. 1982. Paleostress and strain estimates from boudinage structure and their bearing on the evolution of a major Variscan fold-thrust complex in southwest England. *Tectonophysics* **88**, 269–289.

Ferguson, C. C. & Lloyd, G. E. 1984. Extension analysis of stretched belemnites: a comparison of methods. *Tectonophysics* **101**, 199–206.

Ghosh, S. K. & Ramberg, H. 1976. Reorientation of inclusions by combination of pure shear and simple shear. *Tectonophysics* **34**, 1–70.

Hanmer, S. 1986. Asymmetrical pull-aparts and foliation fish as kinematic indicators. *J. Struct. Geol.* **8**, 111–122.

Hara, I. & Umemura, H. 1979. Some considerations on the age of Matsugadaira–Motai metamorphic rocks. In: *The Japanese Islands* (edited by Editorial Committee of the 'Professor Hiroshi Kano Memorial Volume'). Akita University Press, Akita, pp. 559–578 (in Japanese with English abstract).

Hirth, G. & Tullis, J. 1992. Dislocation creep regimes in quartz aggregates. *J. Struct. Geol.* **14**, 145–159.

Hossain, K. M. 1979. Determination of strain from stretched belemnites. *Tectonophysics* **60**, 279–288.

Ida, Y. & Muzutani, H. 1978. Elastic properties of Earth-forming materials. In: *Materials of the Earth* (edited by Akimoto, S. & Mizutani, H.). Iwanami Syoten, Tokyo, pp. 1–100. (Textbook in Japanese.)

Itaya, T. 1978. Notes on petrography and rock-forming mineralogy (3): albite porphyroblasts containing TiO_2-minerals from Sambagawa pelitic schists in central Shikoku, Japan. *J. Japan. Ass. Min. Petrol. Econ. Geol.* **73**, 339–345.

Iwamatsu, A. 1975. Folding-styles and their tectonic levels in the Kitakami and Abukuma mountainous lands, Northeast Japan. *J. Fac. Sci. Univ. Tokyo* **19**, 95–131.

Ji, S. & Mainprice, D. 1988. Natural deformation fabrics of plagioclase: implications for slip systems and seismic anisotropy. *Tectonophysics* **147**, 145–163.

Ji, S. & Zhao, P. 1993. Location of tensile fracture within rigid–brittle inclusions in a ductile flowing matrix. *Tectonophysics* **220**, 23–31.

Kelly, A. 1973. *Strong Solids*. Clarendon Press, Oxford.

Kuroda, Y. & Ogura, Y. 1963. Epidote-amphibolites from the Northeastern Abukuma Plateau, Japan. *Sci. Rept Tokyo Kyoiku Daigaku Sec. C* **80**, 246–268.

Lloyd, G. E. & Ferguson, C. C. 1989. Belemnites, strain analysis and regional tectonics: a critical appraisal. *Tectonophysics* **168**, 239–253.

Lloyd, G. E., Ferguson, C. C. & Reading, K. 1982. A stress-transfer model for the development of extension fracture boudinage. *J. Struct. Geol.* **4**, 355–372.

Maekawa, H. 1988. High P/T metamorphic rocks in Northeast Japan. *Chikyu Kagaku* **42**, 212–219 (in Japanese with English abstract).

Masuda, T. & Fujimura, A. 1981. Microstructural development of fine grained quartz aggregates by syntectonic recrystallization. *Tectonophysics* **72**, 105–128.

Masuda, T. & Kuriyama, M. 1988. Successive 'mid-point' fracturing during microboudinage: an estimate of the stress-strain relation during a natural deformation. *Tectonophysics* **147**, 171–177.

Masuda, T., Michibayashi, K. & Ohta, H. 1995. Shape preferred orientation of rigid particles in a viscous matrix: re-evaluation to determine kinematic parameters of ductile deformation. *J. Struct. Geol.* **17**, 115–129.

Masuda, T., Shibutani, T., Igarashi, T. & Kuriyama, M. 1989. Microboudin structure of piedmontite in quartz schists: a proposal for a new indicator of relative palaeodifferential stress. *Tectonophysics* **163**, 169–180.

Masuda, T., Shibutani, T., Kuriyama, M. & Igarashi, T. 1990. Development of microboudinage: an estimate of changing differential stress with increasing strain. *Tectonophysics* **178**, 379–387.

Misch, P. 1969. Paracrystalline microboudinage of zoned grains and

other criteria for synkinematic growth of metamorphic minerals. *Am. J. Sci.* **267**, 43–63.
Otsuki, M. 1980. Notes on petrography and rock-forming mineralogy (7): zonal structure of albite porphyroblast from basic Sambagawa schists in central Shikoku. *J. Japan. Ass. Min. Petrol. Econ. Geol.* **75**, 196–202.
Ramberg, H. 1955. Natural and experimental boudinage and pinch and swell structures. *J. Geol.* **63**, 512–526.
Ramsay, J. G. 1967. *Folding and Fracturing of Rocks*. McGraw-Hill, New York.
Takagi, K. & Hara, I. 1979. Relationship between growth of albite porphyroblasts and deformation in a Sambagawa schist, Central Shikoku, Japan. *Tectonophysics* **58**, 113–125.
Terasawa, K. 1971. *Sugaku-gairon*. Iwanami, Tokyo. (Textbook of mathematics written in Japanese.)
Tullis, J. & Yund, R. A. 1977. Experimental deformation of dry Westerly granite. *J. geophys. Res.* **82**, 5705–5718.
Tullis, J. & Yund, R. A. 1985. Dynamic recrystallization of feldspar: a mechanism of ductile shear zone formation. *Geology* **13**, 238–241.
Tullis, J. & Yund, R. A. 1987. Transition from cataclastic flow to dislocation creep of feldspar: mechanisms and microstructures. *Geology* **15**, 606–609.
Tullis, J. & Yund, R. A. 1991. Diffusion creep in feldspar aggregates: experimental evidence. *J. Struct. Geol.* **13**, 987–1000.
Vernon, R. H. 1989. Porphyroblast-matrix microstructural relationships—recent approaches and problems. In: *Evolution of Metamorphic Belts* (edited by Daly, J. S., Cliff, R. A. & Yardley, B. W. D). *Geol. Soc. Spec. Pub.* **43**, 83–102.
White, J. C. & Mawer, C. K. 1986. Extreme ductility of feldspars from a mylonite, Parry Sound, Canada. *J. Struct. Geol.* **8**, 133–144.
Yardley, B. W. D. 1989. *An Introduction to Metamorphic Petrology*. Longman, New York.
Zwart, H. J. 1962. Relations between folding and metamorphism in the central Pyrenees, and their chronological succession. *Geol. Mijnb.* **39**, 63–180.

APPENDIX A

Statistically, the true proportion of broken grains (μ) at a certain aspect ratio is estimated with a confidence interval

$$\left(t\sqrt{\frac{f/n(1-f/n)}{n}}\right)$$

as

$$f/n - t\sqrt{\frac{f/n(1-f/n)}{n}} < \mu < f/n + t\sqrt{\frac{f/n(1-f/n)}{n}},$$

where n and f ($0 < f < n$) are the total number of measured grains and the number of broken grains, respectively, and t is Student's t which is related to the size of the critical region and $n-1$ (e.g. Cheeney, 1983). The confidence interval is a function of n, f and t. Taking the size of the critical region as 0.05, we searched critical n. By assuming $f/n = 0.5$, the confidence interval is calculated as 0.234, 0.206, 0.187, 0.129, 0.090 and 0.031 for $n = 20$, 25, 30, 60, 120 and 1000, respectively. Since the confidence interval is maximum when $f/n = 0.5$, these values give the maximum range of uncertainty at each n. Considering these values and the countable number of grains in analysed samples, we chose $n = 25$ as the minimum number of measurements for stress analysis. The actual confidence interval for each aspect ratio is usually less than 0.1, because n is sometimes much larger than 25 and f/n is not 0.5.

The confidence interval of the proportion of broken grains reflects uncertainty in the determination of B. Upper and lower limits of reliability of B were estimated by using values of

$$f/n + t\sqrt{\frac{f/n(1-f/n)}{n}}$$

and

$$f/n - t\sqrt{\frac{f/n(1-f/n)}{n}}$$

instead of f/n at each r in our stress analysis, respectively. At its maximum, B has an uncertainty of ± 0.13; uncertainty is usually less than ± 0.1.

APPENDIX B

Elastic constants of minerals show a weak temperature dependence, and E_q and E_a can be expressed as:

$$E_q = E_{q,273} - \frac{\partial E_q}{\partial T}\Delta T$$

$$E_a = E_{a,273} - \frac{\partial E_a}{\partial T}\Delta T,$$

where $E_{q,273}$ and $E_{a,273}$ are elastic constants of quartz and albite at 0°C, respectively,

$$\frac{\partial E_q}{\partial T} \quad \text{and} \quad \frac{\partial E_a}{\partial T}$$

are their temperature derivatives, and ΔT is the temperature in °C. Therefore, E_q/E_a can be approximated by using the first two terms of a Taylor's series (e.g. Terasawa 1971) as:

$$\frac{E_q}{E_a} \cong \frac{E_{q,273}}{E_{a,273}} + \frac{\frac{\partial E_a}{\partial T}E_{q,273} - \frac{\partial E_q}{\partial T}E_{a,273}}{E_{a,273}^2}\Delta T.$$

Although we do not have exact values of the elastic constants of quartz and albite and their temperature derivatives, we do know the order of magnitude of their values: the elastic constants of silicate minerals are in the order of 10^3 [Kbar] and their temperature derivatives are in the order of 10^{-1} [Kbar K^{-1}] (e.g. Ida & Mizutani 1978). By substituting these values into the above equation, we evaluate that the second term of the above equation is negligibly small compared with the first one. Thus, E_q/E_a can be regarded as a constant in our stress analysis. For similar reasons we neglect pressure dependence on the ratio of elastic constants.